FDR for non destructive evaluation: inspection of external post-tensioned ducts and measurement of water content in concrete

F Visco Comandini, T Bore, G Six, Florence Sagnard, S Delepine Lesoille, G Moreau, D Placko, F Taillade

FDR for non destructive evaluation: inspection of external post-tensioned ducts and measurement of water content in concrete

F. Visco-Comandini[(1)], T. Bore[(2)], G. Six[(1)], F. Sagnard[(1)], S. Delepine-Lesoille[(3)], G. Moreau[(4)], D. Placko[(2)], F. Taillade[(4)]

[(1)] Université Paris Est, Ifsttar, 14-20 boulevard Newton Cité Descartes, Champs sur Marne, 77447 Marne la Vallée Cedex 2, France
[(2)] SATIE, ENS Cachan, CNRS, 61 avenue du président Wilson, F 94 235 Cachan Cedex
[(3)] Andra, 1-7 rue Jean Monet, F- 92298 Chatenay-Malabry France
[(4)] EDF R&D STEP, 6 quai Watier, BP 49, 78401 Chatou, France

Introduction

The water content in concrete (nuclear structures and nuclear waste repositories) is a major topic to understand and predict the behaviour at the end of the operating period. That is the reason why ANDRA and EDF are involved in research programs dedicated to concrete Thermo-Hydro-Mechanical (THM) modeling and to in situ water content assessment technologies [18].

Another example concerns the bridges which include `external_ post-tensioned cables to reinforce these structures. These cables are not into the concrete material, hence potentially accessible for measurement. They are generally placed in High Density Poly-Ethylene (HDPE) ducts, where the residual space is filled under high pressure with a cement grout intended to prevent corrosion. Nevertheless, in some cases, the cables breaking occur in non-protected zones [12, 4] because of the presence of a `white paste_ or grout voids.

To remote diagnosis anywhere and in real time of post tensioned ducts or to measure the water content in concrete, we propose a structural health monitoring method based on Frequency Domain Reflectometry (FDR). Today˘s, advanced reflectometry methods provide an efficient solution for the fault-detection and for their diagnosis in electric transmission lines [21],[22].

This paper presents a direct model of the FDR method based on telegrapher˘s equations. An analysis of these signals, based on scattering theory, enables one to retrieve the impedance distribution of the electric line. The impedance distribution depends on damage into the duct or the water content in concrete. An inversion algorithm is realized with software `ISTL_ provided by INRIA. FDR method has been applied to two real cases: measurement of the water content in concrete and the diagnostic of the external post tensioned duct.

Theorical Background

Cable Model

The post-stressed cable considered here is made of cement, white paste and air.
We characterize each material by the relative complex permittivity $\varepsilon_n = \breve{\varepsilon}_n - j\,\breve{\breve{\varepsilon}}_n$ ($j=\sqrt{-1}$) where n can be air, cement, HDPE or white paste (Table 1).

Material	Permittivities
Air	1
HDPE	2.5
Cement	5
White Paste	63+j2.6/(2)

Table 1 Material's permittivities

The height of each material h_n in the transversal section depends on the position variable $z \in [0,l]$ and d represents the diameter of the cable (see Figure 1).

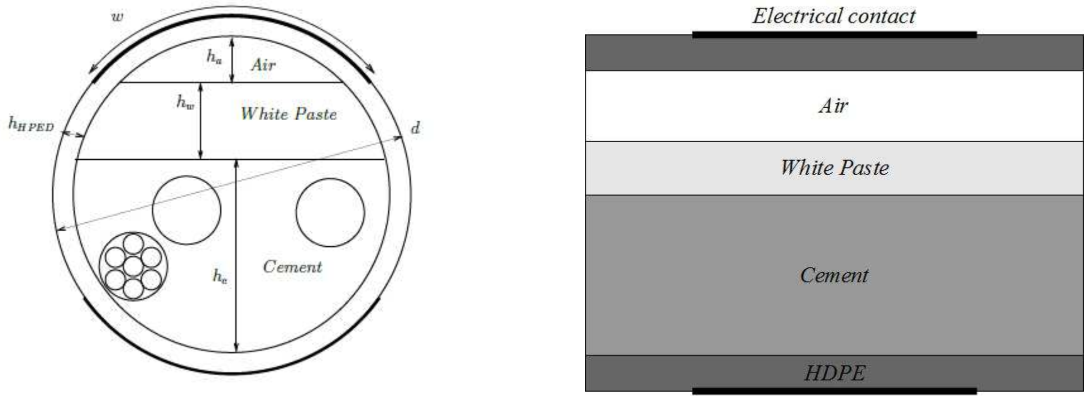

(a) Section of a duct (b) Equivalent electrical model

Figure 1: Cable's reduced model

The principle of our method consists in adding two electrically conductive tapes of width w on the upper and lower parts of the duct. Then, the electric conductors and the ducts form an electrical line between tapes. Given a post-stressed cable, we can calculate an apparent permittivity ε_{app} using the basic formula of a multi-layers planar medium material's permittivity [16]:

$$\frac{1}{\varepsilon_{app}(z)} = \frac{1}{d}\sum_{n} \frac{h_n(z)}{\varepsilon_n(z)}$$

The width w of metallic tape is smaller than the diameter d of tube, so the fringing effect cannot be ignored completely and the assumption about the fields of the parallel plate line is not valid [15].

Electric model of the transmission line

The electric signal transmission is generally modeled using the "telegrapher's equation" and characterized by the line parameters R, L, C and G, representing, respectively, the resistance, the inductance, the capacitance and the shunt conductance.

In the harmonic regime, telegrapher's equations are written as follow:

$$\partial_z V(z,\omega) + (R + jL\omega)\, I(z,\omega) = 0$$
$$\partial_z I(z,\omega) + (G + jC\omega)\, V(z,\omega) = 0$$

where the intensity $I(z,\omega)$ and the voltage $V(z,\omega)$ depend on the space position z and the pulsation $\omega = 2\pi f$ where f is the frequency in a range of frequencies from 1 MHz to 1GHz with the step $\Delta f = 1$ MHz.

The following boundary conditions are verified at both ends at $z=0$ and $z=l$

$$V(0,\omega) + Z_S(\omega)\, I(0,\omega) = V_S(\omega)$$
$$V(l,\omega) - Z_T(\omega)\, I(l,\omega) = 0$$

$Z_S(\omega)$ is the internal source impedance connected at $z=0$ and $Z_T(\omega)$ is the terminal impedance connected at $z=l$. $V_S(\omega)$ represents the harmonic source generator.

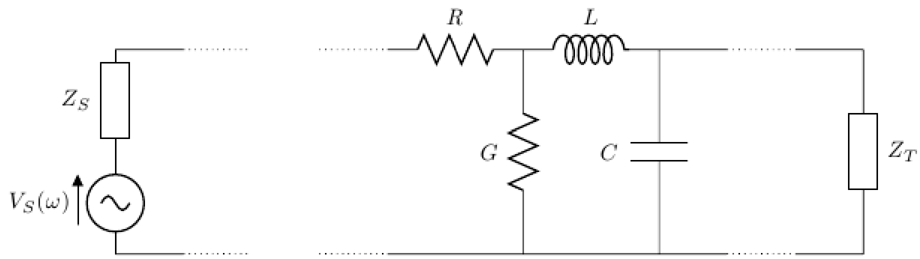

Figure 2: Transmission line model with one source generator

Initially, we assume that cable model (Fig. 1a) is equivalent to a coplanar geometry (Fig.1b). Practical micro-strip lines have width-to-height ratios *w/d<1*. Using the usual design formula [2], the effective dielectric constant of a micro-strip line is given approximately by:

$$\varepsilon_{eff}(f) = \frac{\varepsilon_{eff}(f) + 1}{2} + \frac{\varepsilon_{eff}(f) - 1}{2}\frac{1}{\sqrt{1 + 12d/w}}$$

Line parameters and permittivity/permeability are related through the following formulas (see [16]):

$$L(f) = \mu\frac{d}{w}$$

$$R(f) = \frac{2R_s(f)}{w}$$

$$C(f) = \varepsilon'(f)\frac{w}{d}$$

$$G(f) = \omega\frac{\varepsilon''(f)\,w}{d}$$

where $R_s(f)$ is the surface resistivity of metallic tape.

Direct problem: Riccati Equation

Reflectometry technique consists in exciting a cable with a given signal and analyzing the returning signals, composed by all signals reflected by the heterogeneities of the line. Reflectometry experiments lead to observing voltages and currents as a function of the time at some position: only the traveling times and amplitudes of waves are accessible by such experiments. A fault can only localized in terms of the traveling time of the reflected test wave starting from the test point. It becomes natural to work with the traveling time instead of the spatial coordinates. The traveling time is also called the *electrical distance*.

The *Liouville transformation* allows to transform the spatial coordinate *z* into the electrical distance *x*. The Liouville transformation writes as follow:

$$x(z) = \int_0^z \frac{dz}{v(z)}$$

$x(z)$ corresponds to the wave traveling time from position *0* to *z*.

The electrical distance L=*x(l)* corresponds to the physical length *l* and we will be able to write any function *g(x)≡g(z(x))*.

The wave velocity associated with the complex permittivity is defined as:

$$v(z) = \frac{1}{\sqrt{\mu\,\varepsilon'(z)\,\frac{1 + \sqrt{1 + \tan\delta(z)^2}}{2}}}$$

where $\tan\delta(z) = \varepsilon''(z)/\varepsilon'(z)$.

Reflection coefficient is modeled by a set of Riccati equations.

For a fixed frequency f∈[1MHz,1GHz], the corresponding Riccati equation, denoted by *R*(f) shows the behavior of the reflection coefficient along the line [0,L]. Let us define the high-frequency impedance such as:

$$Z_c(x) = \sqrt{L(x)/C(x)} \qquad (1)$$

then the set of Riccati equations *R*(f)

$$\frac{d}{dx}R_{[illegible]}(x,\omega) = [illegible] + \frac{[illegible]}{[illegible]}\,[illegible]\,R_{[illegible]}^{2}(x,\omega) - \left([illegible] + \frac{[illegible]}{[illegible]}\right)Z_c(x) \qquad (2)$$

$$R_{[illegible]}(L,\omega) = R_L(\omega)$$

where again $\omega = 2\pi f$.

The reflection coefficient $R_{[illegible]}(\omega)$ is defined by

$$\rho_{in}(\omega) = \frac{Z_{in}(0,\omega) - Z_c}{Z_{in}(0,\omega) + Z_c} \quad (3)$$

where Z_c is the internal impedance of source.

The high-frequency impedance $Z_\infty(\omega)$, the loss terms $\frac{G(\omega)}{C(\omega)}$ and $\frac{R(\omega)}{L(\omega)}$ are related to the material permittivity ε.

Taking fringing effects into account, the high frequency impedance is given by [16]

$$Z_\infty(\omega) = \frac{1}{2\pi}\sqrt{\frac{\mu_0}{\varepsilon_0\varepsilon_{eff}(\omega)}}\ln\left(\frac{8h}{w} + \frac{w}{4h}\right)$$

The loss terms can be easily recover through the two wires line parameter's formula (see for example [15]):

$$\frac{G(\omega)}{C(\omega)} = \sigma\frac{\varepsilon''(\omega)}{\varepsilon'(\omega)}$$
$$\frac{R(\omega)}{L(\omega)} = \frac{2\alpha_c(\omega)}{c}$$

Inverse problem: ISTL software

The inversion method is processed by a software "ISTL" (Inverse Scattering Transform Lossless) developed at INRIA[1] by the team SISYPHE. ISTL is based on an inverse scattering method applied to transmission lines [22].

The inverse scattering transform consists of the following steps for computing the profile of $L(x)/C(x)=\varepsilon_{eff}(x)$, from the reflection coefficient $\rho_{in}(\omega)$. See [11] for details.

1. Let the Fourier transform of the reflection coefficient $\rho_{in}(\omega)$ be
$$\Phi(t) = \frac{1}{2\pi}\int_{-\infty}^{\infty}\rho_{in}(\omega)e^{i\omega t}d\omega$$

2. Solve the integral equations (known as Gelfand-Levitan-Marchenko equations) for its unknown kernels $K_1(t,\tau)$ and $K_2(t,\tau)$:
$$K_1(t,\tau) + \int_t^\infty K_2(t,s)\Phi(s+\tau)ds + \Phi(t+\tau) = 0$$
$$K_2(t,\tau) + \Phi(t+\tau) + \int_t^\infty K_2(t,s)\Phi(s+\tau)ds + \Phi(t+\tau) = 0$$

3. Compute the heterogeneity function through
$$\frac{1}{\varepsilon_{eff}(x)}\frac{d}{dx}\varepsilon_{eff}(x) = 2K_1(x,x)$$

Simulations and Validations

In order to validate the proposed method for post-tensioned cable diagnosis, results of numerical simulation are presented in this section. To simulate reflectometry measurements, reflection coefficients are computed by solving the Riccati's equation (2).

In the simulation, we consider a duct filled with cement, white paste and air. A material widths profile (Figure 3) is considered together with the permittivity's values shown in Table 1.

[1] INRIA Institut National de Recherche en Informatique et en Automatique, Domaine de Voluceau-Rocquecourt- 78153 Le Chesnay, France

For each excitation frequency in the reflection coefficient of a duct was calculated using (2) and (3). A profile is simulated in both *z* and *x* coordinates in Figure 3. The simulated reflection coefficient (modulus and phase) is shown in Figure 4.
ISTL software was designed to retrieve the characteristic impedance for a lossless transmission line. Nevertheless, the algorithm is robust and it works also for lossy transmission line, that means it is capable of finding the impedance defined in (1). The profile computed through ISTL is compared to the original simulated profile in Figure 5: oscillations of retrieved impedance are due to the disadaptation of terminal impedance.

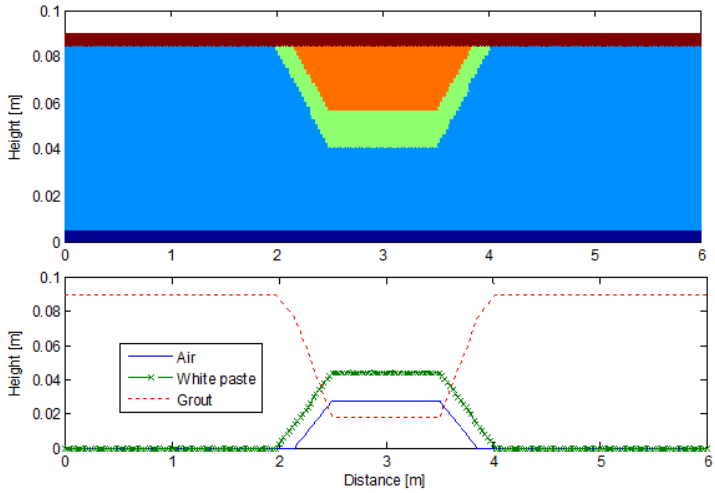

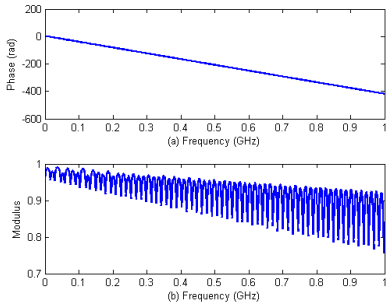

Figure 3: Simulated reflection coefficient

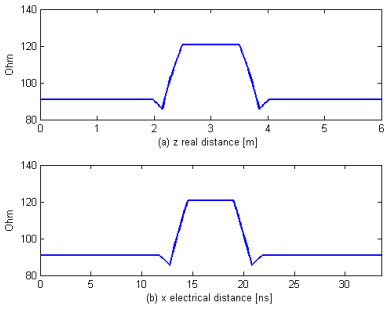

Figure 4: Simulated profile : *z* vs *x*.

We remind that the inverse scattering transform computes the high frequency as a function of *x*. In practice it would be more useful to inspect the ratio as a function of *z*, the true spatial coordinate of the transmission line. Like all reflectometry methods, the information obtained by observing incident and reflected waves is related to the wave propagation time *x*.

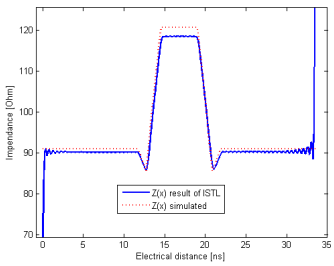

Figure 5: The impedance profile computed by ISTL and compared to the simulated profile

Experimental results

Experimental mockup

Experiments were carried out to check the validity of the numerical simulations.
Two mockup ducts of 6 *m* length and with a diameter of 90 *mm* have been considered. They are equipped with 12 steel cables of 15 *mm* diameter (Figure 6).
These ducts were fixed on a frame reproducing the curvature of pre-tensioned ducts on a stack. The vents are positioned on either side of the top point, i.e. in practice each side of the deviator. Moreover, wooden wedges were inserted between the metal structures supporting the ducts. The cement was injected into duct A using a standard *Superstresscem* with a ratio Water/Cement 0.35. In duct B it has been injected with cement together with a *ChrysoGT* adjutant (Water/Cement 0.65) in order to promote the appearance of white paste.

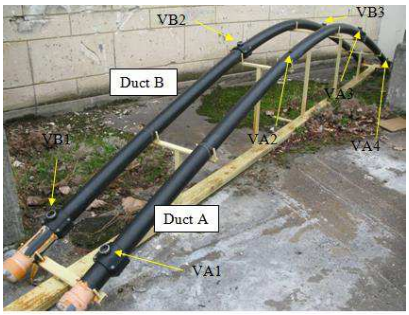

Figure 6: External post stressed duct in Trappes (IFSTTAR laboratoires, France)

□□ measurements are performed using Vector Network Analyzer (VNA) of *Anritsu MS2026*. Ducts are equipped with metal strips on the upper and lower parts of the ducts. The strip is composed of adhesive aluminum rubber (thickness 0,1*mm* and width 50*mm*). This pair of strips is connected to a coaxial cable through clips. The coaxial cable is linked to the VNA port. The measurements are performed on a frequency range of 1 MHz to 1 GHz with a frequency step of 1 MHz (1000 points). The VNA coaxial cable is connected to the duct through clips and at the end of duct another pair of clips connects the metallic strips to known terminal impedance.
On each cable, we performed three different experiences connected to three different terminal impedances branched at the end of the ducts (open circuits, short circuits and an impedance of 50 Ohms).
The ducts have been inspected by hammer auscultation. Figure 7 shows the location of void areas and vents on ducts. Cables have not been open so the exact profile of the heights of materials is not known.

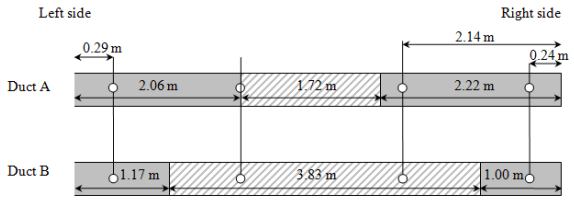

Figure 7: Location of void areas (hatched) and vents (o) on ducts A and B

Data inversion

□□□ measurements of VNA has been fed to "ISTL" software. Results of the inversion software are in Figures 8 and 9. Each figure shows a comparison between three different experiences: the impedance profiles match until the end of the line where the terminal impedances are. ISTL is capable of detecting these three terminations. Both figures shows two bumps of impedance profile at both ends of the cable (around 5 *ns* and 40 *ns*): these variations of impedance correspond to the ruptures of impedance caused by the connection between the coaxial cable and tapes. On the other side, ISTL retrieve the Impedance profile as a function of electrical distance and so it is not able of detecting the physical ends.
From the impedance profile, we deduced the real part of the apparent permittivity and consequently lossless wave velocity. We were able to plot the impedance profiles as functions of physical distance. These inversion results have been compared to hammer auscultation (see Figures 8 and 9). The

presence of void is detected clearly as an increment of the retrieved impedance: we can see a rise of impedance's values in the middle part of duct, where the void is supposed to be.
The oscillations at the beginning of the duct are also due to the ruptures of impedance caused by the connection. Moreover, the vents create a bump of impedance.

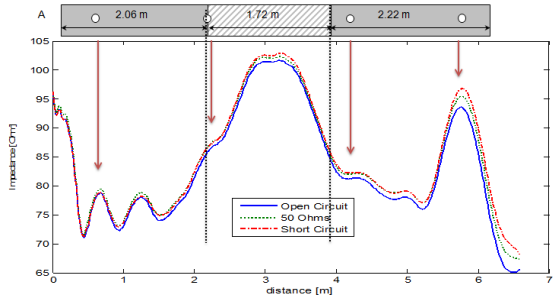

Figure 8: The impedance profile computed by ISTL compared to hammer auscultation on the duct A

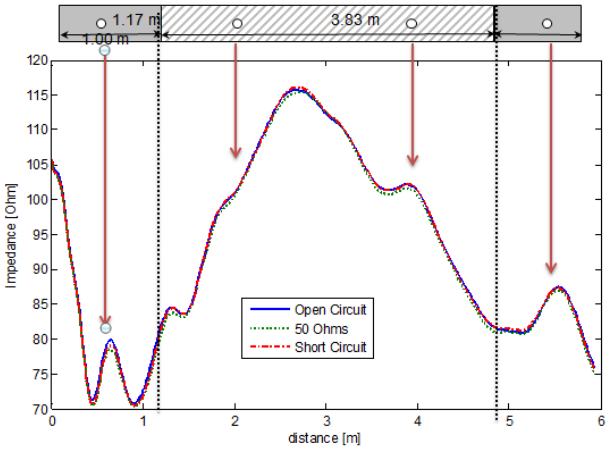

Figure 9: The impedance profile computed by ISTL to hammer auscultation on the duct B

Conclusion and further direction

In this paper, we have presented a new non destructing testing method for external post-tensioned duct based on FDR techniques and we are able to detect the heterogeneities of materials along a cable.
We have developed an equivalent permittivity model, allowing us a reflection coefficient simulation using the telegrapher's model. Theoretical work, taking the properties of the materials and propagation phenomenon into account, enables one to predict the signal measured. We have shown the feasibility of FDR technique of health monitoring post tensioned cables. Details of data measurement used in the feasibility study were explained and validated. We used the software "ISTL" as robust inversion algorithm and these performances are demonstrated in a real case experiment.
In conclusion, this diagnostic method is able to detect the voids along the cable also where it crosses the deviator. Moreover, once the duct equipped with a strip line, the diagnosis can be done remotely to improve the safety of personnel in the event of a cable break. Further research into parametric studies is required in order to detect also the white paste. A quantification of the heterogeneities along the line is needed. An impedance threshold must be found in order to complete the health monitoring process. Another way of research is to apply this method on internal post-tensioned duct.

Acknowledgements

The authors wish to thank the team SISYPHE of INRIA for the development of software `ISTL_.

Bibliography

1) K. Arunachalam, V. R. Melapudi, L. Udpa, and S. S. Udpa, Microwave NDT of cement-based materials using far-field reflection coefficients. NTD & E international, 2006 39 585-593.
2) I. J. Bahl and D. K. Trivedi, A Designer's guide to stripline circuits, MicroWaves, 1977 90-96.
3) E. Blactot, Electrochemical behaviour and corrosion sensitivity of prestressed steel in cement Grout, WIT Transactions on Engineering Sciences, 2007, 54.
4) T. Bore, D. Placko, F. Taillade, M. Himbert, Capacitive sensor for measuring the filled of post-tensioned ducts : experimental set-up, modelling and signal processing, IEEE Sensors Journal, 2012, 13 457-465.
5) X. Dérobert, C. Aubagnac, and O. Abraham, Comparison of NDT techniques on a post-tensioned beam before its autopsy, NDT & International, 2002 35 541-548.
6) A. Dupas, J.P. Sudret, and A. Chabert, Méthode de diagnostic de câbles de précontrainte externe contenus dans des gaines, French Patent n.0107719, 2001.
7) A. Fares and A.K. Alva, Soil water components based on capacitance probes in a sandy soil, Soil Science Society of America Journal, 2002 64 311-318.
8) J. Iaquinta, Contribution of capacitance probes for the inspection of external post-tensioned Ducts, Proceedings of the 16th international conference on NDT, Montreal, 2004.
9) J. B. Jaeger, M. J. Sansalone, and R. W. Poston, Detecting voids in grouted tendon ducts of post-tensioned concrete structures using the impact-echo method, Structural Journal, 1996 93 462-473.
10) O. Jeandupeux, V. Marsico, A. Acovic, P. Fazan, H. Brune, and K. Kern, Use of the scanning capacitance microscopy for controlling wafer processing, Microelectronics Reliability, 2002 42 225-231.
11) G. L. Lamb, Elements of Soliton Theory. John Wiley and sons, 1980.
12) R. Le Roy, Rhéologie et stabilité des matrices cimentaires et des coulis, Etudes et recherches des Laboratoires des ponts et chaussées, LCPC Paris, 2006.
13) I. Matiss, New possibilities of increasing accuracy for non destructive testing. Part 1. Basic principles and application examples. NDT & International, 1999 32 397-401.
14) S.O. Nelson, Measurement and applications of dielectric properties of agricultural products, IEEE Transactions on Instrumentation and Measurement, 1992 41 116-122.
15) S. J. Orfanidis, Electromagnetic waves and Antennas, Rutgers University, 2008.
16) D. M. Pozar, Microwave engineering, Wiley, New York, 3rd ed. edition, 2005.
17) M. Ruprecht, G. Benstetter, and D. Hunt, A review of ULSI failure analysis techniques for DRAMs. Part II: Defect isolation and visualization, Microelectronics Reliability, 2003 4317-41.
18) P. Stephan, J. Salin, Ageing management of concrete structure: Assessment of EDF methodology in comparison with SHM and AIEA guides, Constr. And Build Mat. 2012, 37 924-933.
19) A. Smith, P. Abélard, F. Thummen, and A. Allemand, Electrical characterization as a function of frequency: application to aluminous cement during hydratation, Cement and Concrete Composites, 2002 24 477-478.
20) F. Taillade, C. Aubagnac, C. Lacroix, D. Malaterre, J.-L. Saussol, and L.-M. Cottineau, The capacitive probe: Developing a diagnostic tool for external prestressing ducts, Bulletin des Laboratoires des Pontes et Chaussées, 2008 272 107-122.
21) H. Tang and Q. Zhang, Inverse scattering for lossy electric transmission line soft fault diagnosis, Antennas and Propagation Society International Symposium (APSURSI), 2010.
22) Q. Zhang, M. Sorine, and M. Admane, Inverse Scattering for Soft Fault Diagnosis in Electric Transmission Lines, In 48th IEEE Conference on decision and Control, Shanghai, China, 2009.